Simulation of MEMS devices using linearized compressible flow equations on moving domains

Dominik Mayrhofer[1], Manfred Kaltenbacher[2]

[1] *Institue of Fundamentals and Theory in Electrical Engineering, 8010 Graz, Austria, Email: dominik.mayrhofer@tugraz.at*

[2] *Institue of Fundamentals and Theory in Electrical Engineering, 8010 Graz, Austria, Email: manfred.kaltenbacher@tugraz.at*

Abstract

A new method of sound generation – which we call Advanced Digital Sound Reconstruction (ADSR) – is based on overlapping redirected sound pulses to form an audio signal. The redirection of these sound pulses can be achieved with highly dynamic shutter gates, where multiple cells equipped with shutter gates are actuated consecutively contributing to the overall audio signal. The application of ADSR focuses on Micro-Electro-Mechanical-Systems (MEMS) speakers, hence, simulating such devices requires the consideration of viscous effects. Furthermore, the movement of the shutter gates is vital for the operating principle, therefore, we use the linearized compressible flow equations formulated in an arbitrary Lagrangian-Eulerian (ALE) framework to incorporate all necessary effects. The movement of the domain itself is governed by an artificial quasi-static mechanical computation where a simple forward coupling provides the new geometry for the linearized compressible flow equations. To keep the computational cost minimal, we couple to the acoustic wave equation as soon as viscous effects can be neglected. Finally, the introduced simulation framework is applied to a certain embodiment in order to simulate the operating principle of ADSR and to evaluate the influence of crosstalk between the individual cells generating sound pulses.

Introduction

We investigate an ultrasound pulse-based sound generation principle which we call Advanced Digital Sound Reconstruction [1], with a numerical framework for viscous acoustics on moving domains introduced in [2]. This framework is based on the linearized conservation of mass and momentum in ALE formulation enabling the consideration of viscous effects on moving domains. Including these effects is essential for modeling pump-based sound generation principles like ADSR or micro-pumps in general since viscous effects and domain movement play a significant role for the operating principle [1, 3]. For ADSR, the sound gets generated by overlapping sound pulses stemming from multiple unit cells (UC). We can generate these sound pulses with shutter gates by redirecting sound through two sound ports: a main channel and a side channel. With the help of these shutter gates, a pumping operation of a single UC gets achieved. A schematic overview of such a UC is depicted in Fig. 1. The overall speaker consists of multiple phase-shifted UCs, enabling a smooth audio signal generation. Here, we investigate a simplified model to demonstrate this embodiment's general operating principle and expected cross-talk.

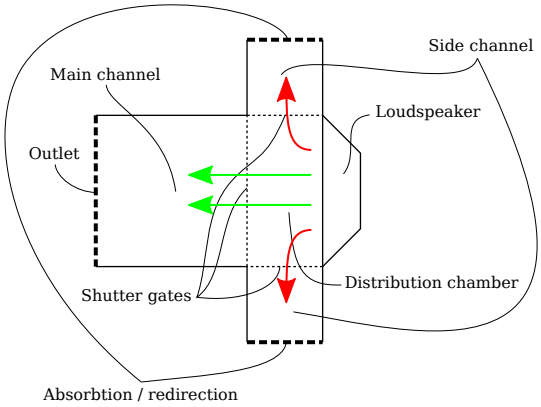

Figure 1: Schematic representation of a single UC.[1]

Governing equations

Based on the framework numerical framework introduced in [2], we briefly recap the governing equations used in the modeling process. In regions where viscous effects and domain movement are essential, we use the linearized conservation of mass

$$\underbrace{\frac{1}{\rho_0 c_0^2}\frac{\partial p}{\partial t} + \nabla\cdot\boldsymbol{v}}_{\text{Standard}} \underbrace{-\frac{1}{\rho_0 c_0^2}\boldsymbol{v}_\mathrm{g}\cdot\nabla p}_{\text{ALE}} = 0 \tag{1}$$

and the linearized conservation of momentum

$$\underbrace{\rho_0\frac{\partial \boldsymbol{v}}{\partial t}}_{\text{Standard}} \underbrace{-\rho_0\boldsymbol{v}_\mathrm{g}\cdot\nabla\boldsymbol{v}}_{\text{ALE}} = \underbrace{\nabla\cdot\left(-p\,[\boldsymbol{I}] + \mu_\mathrm{f}(\nabla\boldsymbol{v} + (\nabla\boldsymbol{v})^\intercal) - \frac{2}{3}\mu_\mathrm{f}(\nabla\cdot\boldsymbol{v})\,[\boldsymbol{I}]\right)}_{\text{Standard}} \tag{2}$$

in ALE form. These equations can be derived by starting from the conservation of mass and momentum in ALE formulation [4] and applying a perturbation ansatz. Throughout this work, the terms linearized compressible flow equations or LinFlow equations will be used synonymously to refer to (1) and (2). In these equations, ρ_0 denotes the mean density, c_0 the speed of sound, p the perturbed fluid pressure, and t the time. Furthermore, $\boldsymbol{v}$ is the perturbed fluid velocity, $\boldsymbol{v}_\mathrm{g}$ the grid velocity, $[\boldsymbol{I}]$ the unit tensor and μ_f the dynamic viscosity. Besides the standard terms, which would also appear for a non-moving formulation, additional ALE-based terms appear in (1) and (2). These terms are additional convective

terms based on the grid velocity, which enable the transport of our primary unknowns over the computational domain. Since the grid velocity can change arbitrarily, the overall weak form includes a solution-dependent parameter. Hence, an iterative forward coupling approach is employed.

Besides the grid velocity, the overall domain movement gets calculated to evaluate the linearized compressible flow equations on the moving domain. Therefore, we use a mesh-smoothing algorithm based on a quasi-static mechanics computation [5]. The advantage of this approach is the high flexibility and robustness of the mesh smoothing since the pseudo-material can be freely adapted to one's needs. The governing equation is given by the quasi-static mechanic solution of

$$-\nabla \cdot ([\boldsymbol{c}] : [\boldsymbol{S}]) = 0, \tag{3}$$

where the strain tensor $[\boldsymbol{S}]$ is defined as

$$[\boldsymbol{S}] = \frac{1}{2} \left(\nabla \boldsymbol{u} + (\nabla \boldsymbol{u})^{\intercal} \right). \tag{4}$$

In these equations, $[\boldsymbol{c}]$ denotes the stiffness tensor and $\boldsymbol{u}$ the displacement vector. The stiffness tensor of rank 4 depends on the chosen material parameters and can be adapted to each problem for the best mesh smoothing results. Solving (3) in a given system will return the updated coordinates required for evaluating the linearized compressible flow equations on the moving domain. Finally, the grid velocity needed for the ALE-specific terms gets calculated using a backwards difference scheme of second order. Due to the chosen approach for modeling viscous effects on moving domains, the computation of a moving section is computationally more involved than, for example, standard acoustics. Therefore, it is advisable to couple to the acoustic wave equation

$$\frac{1}{c_0^2} \frac{\partial^2 p_\mathrm{a}}{\partial t^2} - \nabla \cdot \nabla p_\mathrm{a} = 0 \tag{5}$$

as soon as possible to reduce the computational effort. Whether we use the acoustic potential or pressure formulation is not crucial here. Hence, we only briefly describe the process for the wave equation in pressure formulation, where we solve for the acoustic pressure p_a. To couple to the linearized compressible flow equations, we have to ensure the continuity of surface traction

$$-p_\mathrm{a} \boldsymbol{n} = [\boldsymbol{\sigma}] \cdot \boldsymbol{n} \tag{6}$$

as well as the continuity of the normal acceleration

$$\frac{\partial \boldsymbol{v}}{\partial t} \cdot \boldsymbol{n} = -\frac{1}{\rho_0} \nabla p_\mathrm{a} \cdot \boldsymbol{n}. \tag{7}$$

In (6), $[\boldsymbol{\sigma}]$ denotes the stress tensor, which is included on the right-hand side of (2) and is given by

$$[\boldsymbol{\sigma}] = -p \, [\boldsymbol{I}] + \mu_\mathrm{f} (\nabla \boldsymbol{v} + (\nabla \boldsymbol{v})^{\intercal}) - \frac{2}{3} \mu_\mathrm{f} (\nabla \cdot \boldsymbol{v}) \, [\boldsymbol{I}]. \tag{8}$$

The presented equations now get combined in an iterative forward coupling approach consisting of three major steps:

- Solve (3) to obtain the updated coordinates and grid velocity by applying Dirichlet displacement boundary conditions for the mesh deformation.
- Apply the new coordinates and grid velocity to the computation of (1) and (2) with respect to their boundary conditions, like a no-slip condition on non-excited walls.
- Solve the directly coupled acoustic wave equation as well as the non-moving regions of the linearized compressible flow equations (problem dependent). This workflow has been implemented in *openCFS* [6] and gets used for the model presented in the next section.

Model setup

For the demonstration of the general principle of ADSR, a simplified 2D model of a UC depicted in Fig. 2 has been chosen. This simplified embodiment consists of a membrane, two shutter gates that can move vertically, and a distribution chamber connecting everything. The left shutter is the main shutter responsible for the sound generation for the main channel connected to the ear. The side shutter connects the distribution chamber to the side channel responsible damping/redirection. For the overall speaker, four 90° phase-shifted UCs get combined, which can also be seen in Fig. 3. For the actual simulation, the membrane movement and the shutter movement get prescribed. For the membranes of UC1 to UC4, the excitation displacement can be seen in Fig. 4. It is apparent that the overall stroke of 5 µm gets used for the excitation resulting in a pre-deformed membrane at $t = 0\,\mathrm{s}$. Using the overall stroke maximizes the achievable sound pressure but also increases complexity since the membranes of the cells have to switch their resting position in each half of the audio signal. Since the sound pressure in an infinite channel is directly proportional to the acoustic particle velocity, it is easier to demonstrate the operating principle based on the excitation velocity, which is shown in Fig. 5. As can be seen, the solid line represents the transmitted velocity peak and, therefore, the sound pressure pulse is directed to the main channel. The dashed line represents the redirected part. The pulse excitation itself has a base (carrier) frequency of 96 kHz. Superimposing the transmitted pulses results in a very close

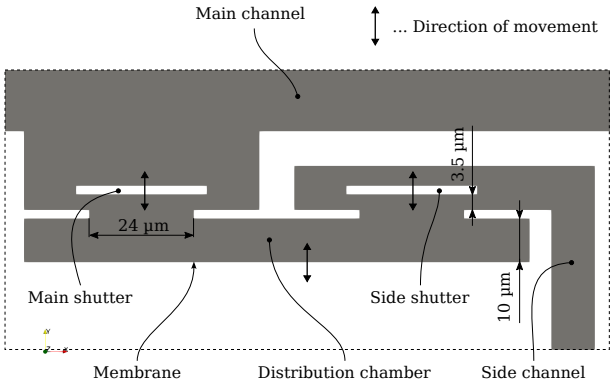

Figure 2: Cut out of a single, simplified UC. The membrane as well as the shutters are moving vertically.

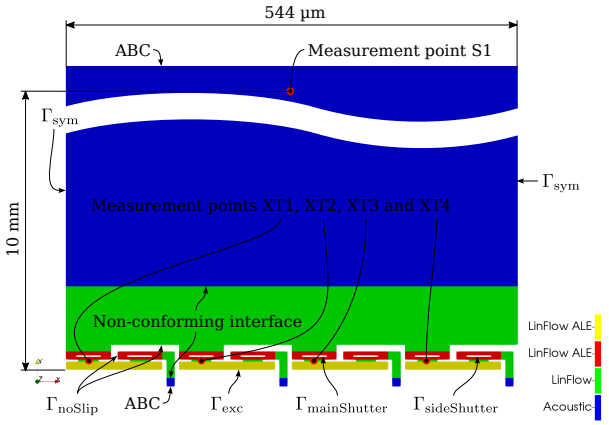

Figure 3: Overall speaker consisting of four UCs. The top and bottom side of the channels is terminated with absorbing boundary conditions (ABCs). At the sides Γ_{sym}, we use a symmetry boundary condition (BC), and at Γ_{noSlip}, a no-slip BC is applied. The surface Γ_{exc} is used to excite the membrane. The boundaries $\Gamma_{mainShutter}$ and $\Gamma_{sideShutter}$ is used to excite the main- and side shutter respectively. A non-conforming interface is used to connect the LinFlow region to the acoustic part for coupling purposes. Finally, multiple measurement points (S1, XT1 to XT4) are defined to evaluate the results.

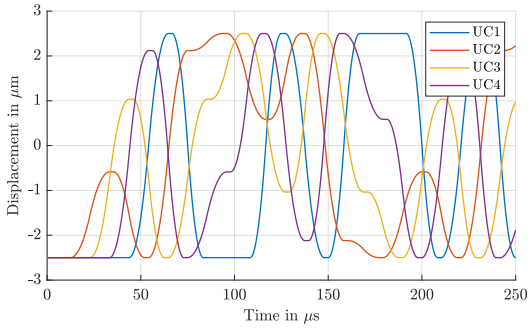

Figure 4: Displacement excitation for the different UCs.

approximation of a sinusoidal audio signal with an audio frequency of $f_a = 6\,\text{kHz}$. Finally, the shutter excitation signal for UC1 is given in Fig. 6, where the 180° phase shift between the main and the side shutter is observable.

Results

In the following section, we present the results for the investigated actuator regarding the general operating principle and the cross-talk.

Operating principle

At first, we show the results for the general operating principle. Therefore, the sound pressure gets evaluated at the measurement point S1, where the results can be seen in Fig. 7. The sound pressure recorded at S1 shows that the operating principle is working as intended since the audio frequency of $f_a = 6\,\text{kHz}$ is visible. Additionally, one can see that the signal is quite noisy due to the shutter mechanism itself. The vertical shutter has the inherent disadvantage of acting as a membrane, resulting in a lot of ultrasound noise due to the shutter opening

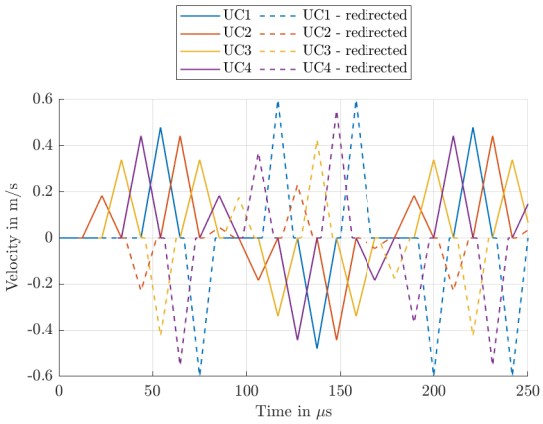

Figure 5: Excitation velocity for all four UCs. The theoretically transmitted and redirected part is marked with solid and dashed lines, respectively.

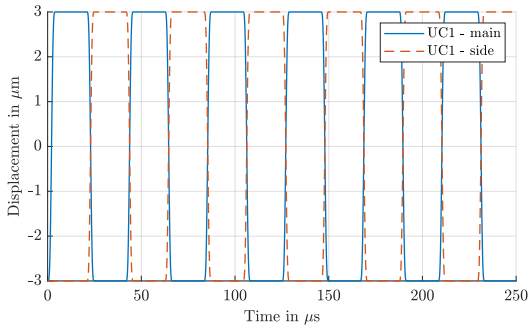

Figure 6: Displacement excitation of the shutters of UC1. The main shutter and the side shutter are 180° phase shifted.

and closing. Performing a FFT of the sound pressure at S1 depicts this behavior even more clearly, which can also be seen in Fig. 8. Here, the audio frequency f_a, the carrier frequency f_c, and its higher harmonics are nicely visible. The only other principle-based contributions to the spectrum are located at $n\,f_c \pm f_a$, where n is an integer ≥ 1 representing the higher harmonics. Since the rest of the spectrum can be considered noise floor, it is safe to say that at a certain distance from the speaker, the only noise generated in this case is ultrasound noise.

Cross-talk

Finally, we evaluate the cross-talk between the individual UCs. Therefore, two simulations have been carried out. In the first one, only UC1 is operated, as in the previous example, and all other UCs stay at their equilibrium (zero) position. Nevertheless, all shutters from UC1 to UC4 are moving. The second simulation only considers the shutter movement. Hence, all membranes stay at their equilibrium position. To evaluate the cross-talk, the resulting sound pressure of the shutter-only simulation is subtracted from the simulation with UC1 active. The resulting sound pressure for the four measurement points can be seen in Fig. 9. The results show that minor differences in the sound pressure signal for XT1 are visible during the switching process. This effect appears because the membrane moves for one simulation but not

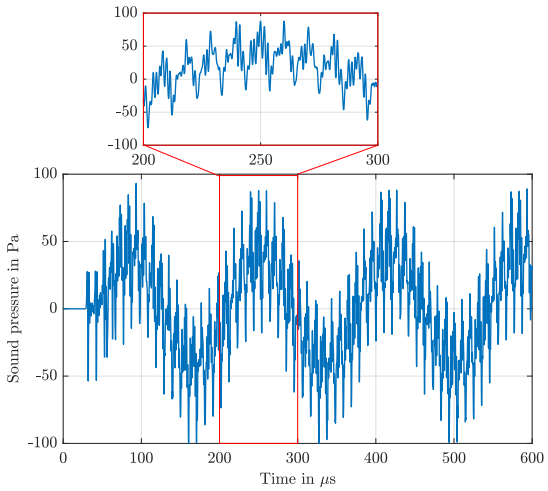

Figure 7: Sound pressure evaluated at S1 with a close-up of the noise generated by the vertical shutter.

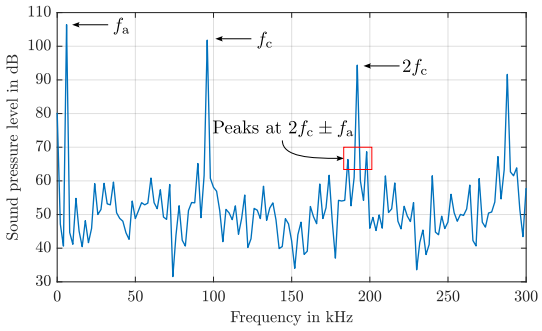

Figure 8: FFT of the sound pressure at S1. Three periods of the audio signal are taken into account.

for the other. Therefore the distribution chamber volume differs over time. Since the back volume varies, the sound will also get reflected earlier or later, depending on the current state, resulting in the highlighted differences. Additionally, some cross-talk can be seen for the positions XT2 to XT4. The close-up in Fig. 9 shows that when the main shutter is open, the shutter noise can propagate into the distribution chamber, which gets picked up by the measurement points. When the main shutter closes, the noise gets suppressed. Hence, the closed main shutter can reduce the noise in the distribution chamber to a very low level. This effective noise reduction also means that the actual leakage (air passing through the speaker from one channel to the other) is close to zero since one shutter is always closed except when the transition from open to closed and vice versa happens. Although some sound can enter the distribution chamber, it can not leave it due to the sealed back side. Almost no noise will enter the distribution chamber when the main shutter is closed. Nevertheless, slight leakage is expected during the transition, which highly depends on the embodiment.

Discussion

Based on a multi-physical model including viscous effects on moving domains, the general principle of an ultrasound pulse-based loudspeaker has been simulated. For the simulation the linearized compressible flow equations

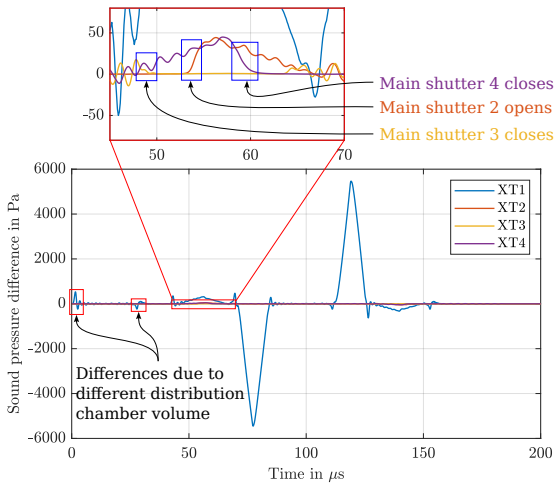

Figure 9: Cross-talk between the UCs (simulation including all shutters and no UCs subtracted from a simulation where UC1 and all shutters are active).

in ALE formulation have been used. The results show that the workflow is well suited for complex simulations of MEMS actuators where domain movement and viscous effects are significant. Furthermore, the presented embodiment has been evaluated regarding the overall operating principle and the resulting noise emissions from the shutter. Additionally, the cross-talk between the individual UCs has also been discussed. The cross-talk itself is already relatively low for the presented embodiment, whereas the ultrasound noise could be reduced by using different shutter principles.

References

[1] D. Mayrhofer and M. Kaltenbacher: A New Method for Sound Generation Based on Digital Sound Reconstruction. Journal of Theoretical and Computational Acoustics , Vol. 29, No. 04 p. 2150021 (2021-12)

[2] D. Mayrhofer and M. Kaltenbacher: Modeling and numerical simulations of MEMS shutter devices. Proceedings of WCCM-APCOM Congress 2022 (Yokohama, Japan, 2022)

[3] A. Aboubakri, V. E. Ahmadi, A. Koşar: Modeling of a Passive-Valve Piezoelectric Micro-Pump: A Parametric Study. Micromachines , Vol. 11, No. 8 (2020)

[4] J. Donea, A. Huerta, J.-Ph. Ponthot and A. Rodríguez-Ferran: Arbitrary Lagrangian–Eulerian Methods. Encyclopedia of Computational Mechanics 14. John Wiley & Sons, Ltd (2004)

[5] G. Link, M. Kaltenbacher, M. Breuer and M. Döllinger: A 2D finite-element scheme for fluid–solid–acoustic interactions and its application to human phonation. Computer Methods in Applied Mechanics and Engineering , Vol. 198, No. 41 (2009) p. 3321-3334

[6] M. Kaltenbacher: openCFS. `https://www.opencfs.org`, ver. 22.02 (2022)